




Role of the Oceanic Vertical Thermal Structure in the Modulation of Heavy Precipitations Over the Ligurian Sea

A. N. MERONI,¹  L. RENAULT,^{2,3} A. PARODI,⁴ and C. PASQUERO¹

Abstract—The importance of the upper ocean thermal vertical structure (mixed-layer depth and stratification) in the control of the precipitation during a heavy-rain-producing mesoscale convective system is investigated by means of numerical simulations. In particular, the fully compressible, nonhydrostatic Euler equations for the atmosphere and the hydrostatic Boussinesq equations for the ocean are numerically integrated to study the effect of the ocean–atmosphere coupling both with realistic initial and boundary conditions and with simpler, analytical vertical temperature profile forcing. It is found that the action of the winds associated with the synoptic system, in which the heavy precipitation event is embedded, can entrain deep and cold water in the oceanic mixed layer, generating surface cooling. In the case of a shallow mixed layer and strongly stratified water column, this decrease in sea surface temperature can significantly reduce the air column instability and, thus, the total amount of precipitation produced.

Key words: Heavy precipitation events, mesoscale convective systems, air–sea interactions, coupled numerical simulations.

1. Introduction

The Mediterranean Basin is a semienclosed sea with high orography surrounding it. The presence of such mountains near the coasts impacts the coastal meteorology and ocean dynamics through intense air–sea exchanges, due to interaction of cold dry continental winds with warm moist air over the sea

(Flamant 2003; Lebeauin Brossier and Drobinski 2009).

Such strong and complex interactions among land, air, and sea are known to produce heavy precipitation events (HPEs) that are characterized by small spatial (10–100 km) and temporal (hours) scales (Ducrocq et al. 2014). Often, these heavy rainfalls are produced by mesoscale convective systems (MCSs), in which deep convective cells re-form in the same position for several hours (Schumacher and Johnson 2005, 2008, 2009). Typically, this happens because warm, moist, and conditionally unstable air hits a colder and drier continental air mass, generating low-level wind convergence that feeds the convective system (Duffourg et al. 2016; Fiori et al. 2017). Such HPEs, then, are often responsible for severe hydrological responses (Gaume et al. 2009; Llasat et al. 2013), which can be catastrophic and cause important economic losses and even casualties (Nuissier et al. 2008).

Previous works have studied the effect of increasing the horizontal resolution of the sea surface temperature (SST) used to force atmospheric numerical simulations of HPEs (Millán et al. 1995; Pastor et al. 2001; Lebeauin et al. 2006; Cassola et al. 2016), finding that, generally, finer-resolution SST fields improve the total precipitation forecast. Using an atmospheric numerical model, Pastor et al. (2001) and Lebeauin et al. (2006) showed that the mean SST over a certain area not too far from the precipitation event controls the amount of rain and that the SST structure modulates the precipitation. In particular, variations in the average SST value modify the surface air stability and the intensity of the warm low-level jet, which is often responsible for the intensity of the precipitation in such events. Warmer

¹ Department of Earth and Environmental Sciences, University of Milano-Bicocca, Milan, Italy. E-mail: agostino.meroni@gmail.com

² Department of Atmospheric and Oceanic Sciences, University of California, Los Angeles, CA, USA.

³ Laboratoire d'Étude en Géophysique et Océanographie Spatiale, CNRS/IRD/UPS/CNES, Toulouse, France.

⁴ CIMA Research Foundation, Savona, Italy.

average SST moistens and heats up the marine boundary layer, which becomes more unstable and can trigger larger rainfalls. A similar dependence of the intensity of an extreme storm on the average SST in the Mediterranean Sea was also found by De Zolt et al. (2006). Instead, the presence of fine-structure SST features, on the km scale, has been shown to play a minor role in terms of the total cumulated precipitation, but to substantially improve the spatial structure of the local heat fluxes, especially in an atmosphere–ocean coupled setup (Carniel et al. 2016; Ricchi et al. 2016, 2017). Moreover, Miglietta et al. (2017) found that small positive SST anomalies can also dramatically increase the risk of tornadic supercells in the southern Mediterranean. On the contrary, a work by Stocchi and Davolio (2017) indicated that the mean SST does not markedly influence the atmospheric water budget over the Adriatic Sea but mainly affects the stability of the planetary boundary layer and orographic flow regimes and, as a consequence, precipitation. More on the role of the SST horizontal structure in influencing the atmospheric boundary layer in a preconvective setup is contained in a related paper (Meroni et al. 2018). There, it is found that the atmosphere responds to SST structures over relatively short temporal and spatial scales, on the order of $O(h)$ and $O(1\text{--}10\text{ km})$, respectively. Thus, through the control of the surface wind convergence, the SST structure is suggested to be a possible factor controlling the position of the heavy rain. The focus of the present study is to understand the role of the oceanic thermal vertical structure in the control of the HPE, which has already proved to be of interest in the region (Lionello et al. 2003; Small et al. 2011, 2012). To this end, we use an ocean–atmosphere coupled model.

In one of the first coupled model experiments for this geographical area, Lebeaupin Brossier et al. (2013) showed how the coupled dynamics can be particularly important in some events. In their case study, the ocean dynamics connects two events that would be independent from an atmospheric point of view. In fact, the surface cooling associated with the enhanced air–sea fluxes and with the vertical mixing between mixed-layer water and deeper (and colder) waters during a mistral event reduces the upper ocean

heat content available for the subsequent HPE, thus reducing the total precipitation compared with an uncoupled case. Berthou et al. (2015), using numerical simulations similar to those of Lebeaupin Brossier et al. (2013), strengthened the role of the ocean in connecting strong wind events with HPEs. In particular, they showed that there are heavy precipitation events in which submonthly atmosphere–ocean coupling mechanisms, such as the SST cooling after a mistral event, play a significant role in controlling, for example, the rainfall location.

At different latitudes, a very interesting negative feedback mechanism takes place at the air–sea interface below tropical cyclones: the intense winds of the cyclonic system entrain cold water from the base of the oceanic mixed layer, which reduces the enthalpy fluxes at the sea surface and reduces the intensity of the cyclone itself (Schade and Emanuel 1999; Vincent et al. 2012; Mei et al. 2015).

The goal of this study is to explore whether a similar mechanism takes place in the midlatitude systems that lead to heavy-rain-producing MCSs. In particular, the hypothesis is that the intense winds of the synoptic system that drives the MCS, by cooling and deepening the oceanic mixed layer in the days preceding the HPE (which is the time scale of the passage of a storm), can reduce the SST, which, in turn, can reduce the precipitation.

Three-dimensional numerical simulations, in both atmosphere-only and ocean–atmosphere coupled configurations, were run to study a HPE due to a MCS at midlatitudes, in Liguria, which is a region in the Northwest of Italy where multiple HPEs of this kind have been observed in the past few years (Rebora et al. 2013; Buzzi et al. 2014; Fiori et al. 2014, 2017; Cassola et al. 2015, 2016). In particular, the focus is on the 9 October 2014 event, which hit the Bisagno catchment and the City of Genoa (Faccini et al. 2015; Silvestro et al. 2016; Cassola et al. 2016; Fiori et al. 2017; Lagasio et al. 2017), causing a flash flood that was responsible for one casualty and damage worth up to roughly €100M.

It is important to underline that the goal of this study is not to reproduce the observed event, but to study the sensitivity of a realistic HPE to the upper ocean thermal vertical structure. In Sect. 2, the setup of the different numerical simulations is described.

Section 3 is devoted to analysis of the effect of the ocean–atmosphere coupling in the event studied using fine scale and realistic initial and boundary conditions. In Sect. 4, instead, the role of the mixed-layer depth (MLD) and oceanic stratification is analyzed by means of coupled numerical simulations forced with simpler oceanic vertical temperature profiles, while Sect. 5 presents the discussion and conclusions.

2. Setup of the Numerical Simulations

Two numerical models, the Weather and Research Forecast (WRF) model with its Advanced Research WRF (ARW) dynamical core version 3.6.1 (Skamarock et al. 2008) and the Regional Ocean Modeling System (ROMS) in its Coastal and Regional Ocean Community (CROCO) version (Penven et al. 2006; Debreu et al. 2012), were coupled to investigate the role of the oceanic vertical thermal structure in the modulation of the precipitating event. WRF solves the nonhydrostatic fully compressible Euler equations on an Arakawa C-grid with mass-based terrain-following coordinates. ROMS is a three-dimensional, free-surface, split-explicit, sigma-coordinate ocean model and was used in its hydrostatic mode.

2.1. Atmospheric Model Configuration

For the atmospheric component, a three-domain two-way nested preparatory simulation was run with WRF standalone (Fig. 1, left panel). It was initialized and forced at the boundary every 3 h with the fields of the European Centre for Medium-Range Weather Forecasts (ECMWF)-Integrated Forecast System (IFS) numerical weather prediction (NWP) model (Simmons et al. 1989), which has horizontal resolution of 0.125° . In particular, this forcing product is a combination of analysis (at 0000 UTC every day) and short-range forecast fields (during the day). The simulation runs for 4 days, from 0000 UTC 06 October 2014 to 0000 UTC 10 October 2014.

The largest domain, d01, is the EURO-CORDEX one (Jacob et al. 2014) and has resolution of 12 km. The intermediate domain, d02, covers the entire

western Mediterranean Basin, most of Southern Europe, and North Africa with resolution of 4 km. The smallest domain, d03, which has resolution of 1.4 km, covers the Ligurian Sea, where the events of interest happened (Fig. 1). In the vertical direction, the grid has 84 levels, as in Fiori et al. (2014), and the cylindrical equidistant projection with a rotated North Pole is used.

The physical parameterizations, chosen according to previous sensitivity experiments in a very similar setup (Fiori et al. 2014), were as follows: the WRF single-moment 6-class scheme (WSM6, Hong and Lim 2006) for the microphysics, the Mellor–Yamada–Nakanishi–Niino level 2.5 option (Nakanishi and Niino 2006, 2009) for the planetary boundary layer, the Tiedtke option (Tiedtke 1989; Zhang et al. 2011) for the cumulus parameterization activated only on the largest domain (d01), the rapid radiative transfer model (RRTM) longwave scheme (Mlawer et al. 1997) and the Goddard shortwave scheme (Chou and Suarez 1999; Chou et al. 2001) for the radiative fluxes, the five-layer thermal diffusion scheme (Dudhia 1996) for the land surface, and the revised MM5 similarity scheme (Beljaars 1995) for the surface layer. Vertical diffusion was performed with a three-dimensional turbulent kinetic energy closure scheme that mixes the full fields and not only the perturbation fields.

2.2. Oceanic Model Configuration and Spin-up

For the oceanic counterpart, a spin-up simulation with ROMS standalone was run for 3 weeks before the event, starting from 0000 UTC 15 September 2014. The Mediterranean Forecasting System product (Oddo et al. 2009) was used as initial and lateral forcing, while the surface forcing came from the ECMWF-IFS NWP model (Simmons et al. 1989), as for the atmospheric model, and provides the momentum, heat, and freshwater fluxes. The ocean was forced at the lateral boundaries every day and at the surface every 3 h. The ocean grid had the same horizontal spatial resolution as the atmospheric one, i.e., 1.4 km. It was slightly smaller than the atmospheric grid over the sea to remove the atmospheric buffer zone (345×262 grid points for ROMS instead of 358×370 as in WRF), as shown in Fig. 1b. In the

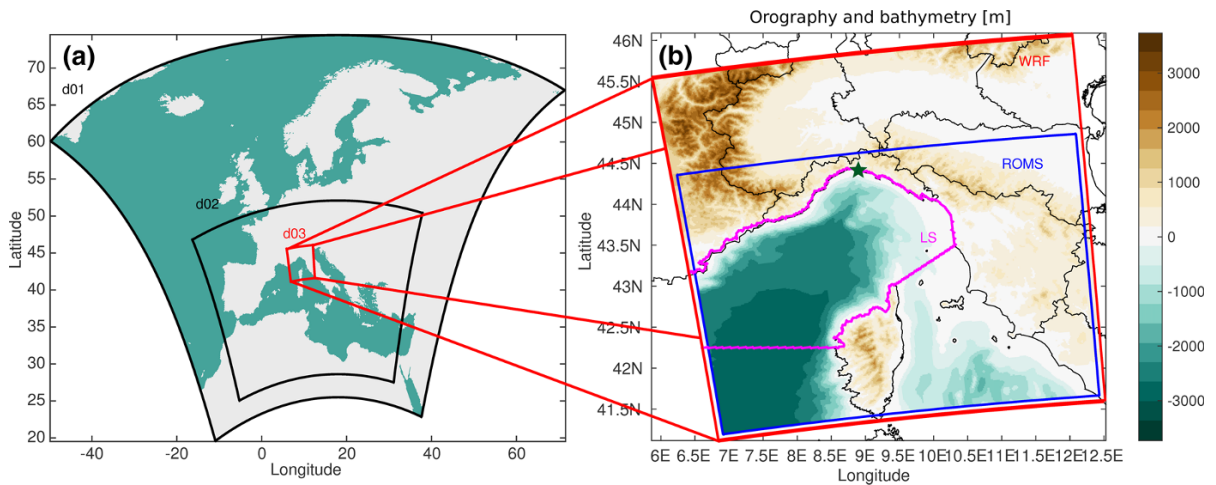


Figure 1

Left panel: the three domains (d01, d02, and d03) used in the double-nested preparatory WRF simulation. Right panel: in red the extension of the WRF domain used in CNTRL, CPLD, UNIF, and L*_M*_sea simulations, that corresponds to the d03 domain of the preparatory simulation; in blue the extension of the ROMS domain used in the coupled simulations, CPLD, and L*_M*_sea. The false colors show the orography and the bathymetry of the domains in meters. The Ligurian Sea (LS), which is a region over which some diagnostics are defined in the text, is highlighted in magenta. The green star denotes the position of the City of Genoa

vertical, the grid was made of 60 levels, with finer vertical resolution near the free surface according to the algorithm of Shchepetkin and McWilliams (2009), with the following stretching parameters: $h_{\text{cline}} = 250$ m, $\theta_b = 2$, and $\theta_s = 7$.

The bathymetry was obtained from the Shuttle Radar Topography Mission global bathymetry and elevation data at 30 arcsec resolution with data voids filled (SRTM30_PLUS) dataset (available at http://topex.ucsd.edu/WWW_html/srtm30_plus.html). This product is based on the 1-min resolution Sandwell and Smith (1997) global dataset. To avoid aliasing and ensure smooth bathymetry in the grid model, a Gaussian filter was applied to the input SRTM30_PLUS data. A second filter was then applied on the topography where its steepness exceeded a threshold value $r = 0.2$. This was done to avoid errors in the pressure gradient computations due to steep bathymetric slope in shallow region with terrain-following coordinates (Beckmann and Haidvogel 1993). Radiative open boundary conditions for baroclinic velocities and tracers were imposed on the western and southern sides (Orlanski 1976; Raymond and Kuo 1984).

Lateral advection was integrated with a third-order upstream scheme (Shchepetkin and

McWilliams 1998) for momentum and with a split and rotated third-order upstream scheme for tracers (Marchesiello et al. 2009; Lemarié et al. 2012). This reduces the spurious diapycnal mixing that would occur along the sigma level and is, thus, suitable for realistic applications with variable bathymetry. Vertical advection, instead, was done with a semiimplicit scheme both for momentum and for tracers (Shchepetkin 2015). Turbulent mixing was represented using the Smagorinsky parameterization in the horizontal (Smagorinsky 1963) and with the nonlocal K-profile parameterization in the vertical (Large et al. 1994). The selected nonlinear equation of state is described in Shchepetkin and McWilliams (2003), being a modified version of that described in Jackett and McDougall (1995).

The choice of the duration of the spin-up was based on the work of Juza et al. (2016), where a 3-week spin-up was considered to be a compromise between the time necessary for complete development of the model's own high-resolution dynamics and a shorter time period that allows better reflection of the observations. Since the domain used in Juza et al. (2016) had similar horizontal resolution (1.8–2.2 km), the choice of a 3-week spin-up is justified. The spin-up was not run in coupled mode,

mostly because of numerical constraints. An ocean-only spin-up, then, with the use of the ECMWF-IFS product, ensures that drifts of the model are avoided, thanks to the assimilation procedure included in the forcing product.

2.3. Numerical Simulations

All simulations were initialized at 0000 UTC 06 October 2014 and run for 4 days, up to 0000 UTC 10 October 2014, in a single WRF domain (d03 of the preparatory simulation described above), coupled to the ROMS domain, when needed (Fig. 1, right panel). The atmospheric initial and boundary conditions were all obtained from the output files of the intermediate domain, d02, of the preparatory simulation described in Sect. 2.1 using the NDOWN tool (Skamarock et al. 2008). Four model configurations were considered. They differ from one another in the initial SST field, in whether they are coupled or not, and for the coupled ones, in the structure of the initial and lateral vertical temperature forcing, as explained below:

The simulation CNTRL was not coupled to the ocean model and was forced at the surface with the SST field obtained from the last output of the ROMS spin-up simulation at 0000 UTC 06 October 2014. The SST was then kept constant until the end.

In the simulation CPLD, WRF was coupled to the ocean model through the Ocean Atmosphere Sea Ice Soil coupler version 3.0 (OASIS3) (Valcke 2013). Every hour, the two models exchanged the following fields: ROMS produced the SST and the surface currents for WRF, and WRF sent to ROMS the freshwater, heat, and momentum fluxes estimated using the COARE bulk formulae (Fairall et al. 2003). In particular, the surface fluxes were determined by the COARE formulation over the sea and by the revised MM5 similarity theory over land. The ocean initial conditions were obtained from the ROMS-alone spin-up simulation, as in Sect. 2.2.

The simulation UNIF was run with WRF standalone and had a homogeneous SST field, equal to the horizontal average over the sea of the SST of the CNTRL simulation, which was, here, not allowed to evolve in time. If $SST_0(x, y)$ is the initial field of the CNTRL simulation, its horizontal average is simply

$$\overline{SST} = \frac{1}{|\Omega|} \iint_{\Omega} dx dy SST_0(x, y) = 22.58^{\circ}\text{C}, \quad (1)$$

where Ω is the region of the domain occupied by the sea and $|\Omega|$ its area.

Finally, the series of simulations $L^*_M^*_{sea}$ were coupled to ROMS, using the same homogeneous initial SST field as the UNIF case, $\overline{SST} = 22.58^{\circ}\text{C}$, while they differed in the two parameters that define the vertical temperature profile of the initial and boundary conditions. In particular, the idealized potential temperature profile prescribed everywhere in the domain at the beginning of the simulation and at the open boundaries during the run was of the form

$$\theta(z) = \begin{cases} \theta_{ML} & \text{for } z > M \\ (\theta_{ML} - \theta_d) \exp[(z - M)/L] + \theta_d & \text{for } z_b < z < M, \end{cases} \quad (2)$$

where the depth z is negative below the sea surface down to the bottom topography value z_b , $\theta_{ML} = \overline{SST}$ is the mixed-layer temperature, and $\theta_d = 12.84^{\circ}\text{C}$ is representative of the temperature at depth in the domain considered (taken from the CPLD simulation). Thus, these simulations differed in the values of M , the initial MLD, and L , the e-folding length of the exponential profile. The name of the simulations contains the values of these two parameters in meters: for example, a simulation named $L5_M25_{sea}$ is characterized by a decaying e-folding length of 5 m and an MLD of 25 m. Following the climatology of D'Ortenzio et al. (2005), which shows that in the Ligurian Sea in October the average MLD is between 15 and 30 m deep, the values of M were chosen to vary between 5 and 35 m, with two possible values of L , 5 m and 35 m. Figure 2 shows four examples of potential temperature profiles used to force the appropriate $L^*_M^*_{sea}$ simulations. The salinity was imposed to be equal to 38.25 psu, which corresponds to 38.43 g kg^{-1} in units of absolute salinity, everywhere in the basin at the beginning of the simulations and, then, along both open boundaries (south and west). These simple temperature and salinity vertical profiles, defined using parameter values relevant to the setup considered, were used both as initial conditions and as lateral forcing along the southern and western open boundaries.

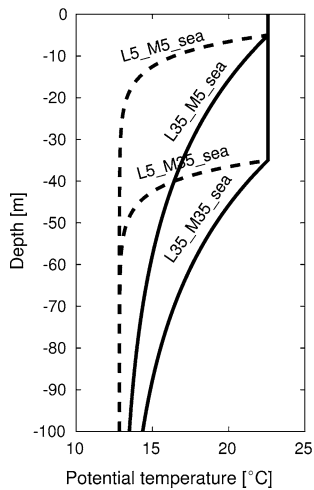


Figure 2

Examples of potential temperature profiles used to force the simulations indicated in the figure

In all these simulations (CNTRL, CPLD, UNIF, and $L^*_M^*_sea$), the parameterization options were the same as described in the previous Sects. 2.1 and 2.2, both for the atmospheric model and for the oceanic one. A summary of the configurations of the numerical experiments containing the initial SST field and the switch for the coupling is presented in Table 1.

3. Effect of the Ocean–atmosphere Coupling

The synoptic conditions leading to the 9th October HPE are well described by Cassola et al. (2016) and Fiori et al. (2017). They mainly consisted of an upper-level trough over the Atlantic Ocean, near Ireland, which produced a low-level flow blowing from the south over the Gulf of Genoa. On the 9th

October 2014, a relatively cold and dry air mass flowing over the Gulf of Genoa from the land played the role of a virtual orographic step, so that the warmer and more humid low-level jet blowing over the sea could overcome its level of free convection, generating the heavy-rain-producing MCS under study (Fiori et al. 2017).

Since the goal of this work is not to develop a more accurate forecast of the HPE, the CNTRL simulation was taken as reference, even though it is known to differ from reality in terms of a couple of issues. In particular, it underestimates the total volume of rain and it simulates the rain over the land only, and not over the sea, as observed. The reasons why no rain is simulated over the sea are to be found in the time of initialization of the model. Other works (Cassola et al. 2016; Fiori et al. 2017; Lagasio et al. 2017) and other simulations run by the authors but not shown here, in fact, are able to capture the triggering of the precipitation over the sea, by initializing the simulations either at midnight of the day of the event or on the day before. In the present work, the choice of initializing the simulations 3 days before the event was made to let the sea respond to the wind forcing of the synoptic system associated with the MCS. This enables one to study the effects that the ocean dynamics have on the precipitation, to the detriment of the forecast. In fact, because of the chaotic nature of the atmospheric system, the realization of the heavy precipitation event in the simulations differs from the observations. But the WRF model is run in a realistic configuration, so that it contains all the physics needed to study the process of interest.

The related paper, Meroni et al. (2018), gives a more detailed description of the simulated event, while here, only the features relevant to the discussion about the ocean coupling are introduced. In particular, Fig. 3 shows the maps of the total precipitation cumulated on the 9th October 2014 in the CNTRL simulation (left panel) and the CPLD one (right panel). It is clear that the coupling with the fully resolved ocean dynamics does not have a relevant impact on the precipitation field cumulated over 24 h.

In Fig. 4, one can see the hourly precipitation rate integrated over the entire domain as a function of

Table 1

Summary of the simulations of interest

Name	Initial SST	Coupling
CNTRL	$SST_0(x, y)$	No
CPLD	$SST_0(x, y)$	Yes
UNIF	\overline{SST}	No
$L^*_M^*_sea$	\overline{SST}	Yes

$SST_0(x, y)$ was obtained from the ROMS spin-up simulation as described in the text, and \overline{SST} is the horizontal average of the $SST_0(x, y)$ field, as in Eq. 1

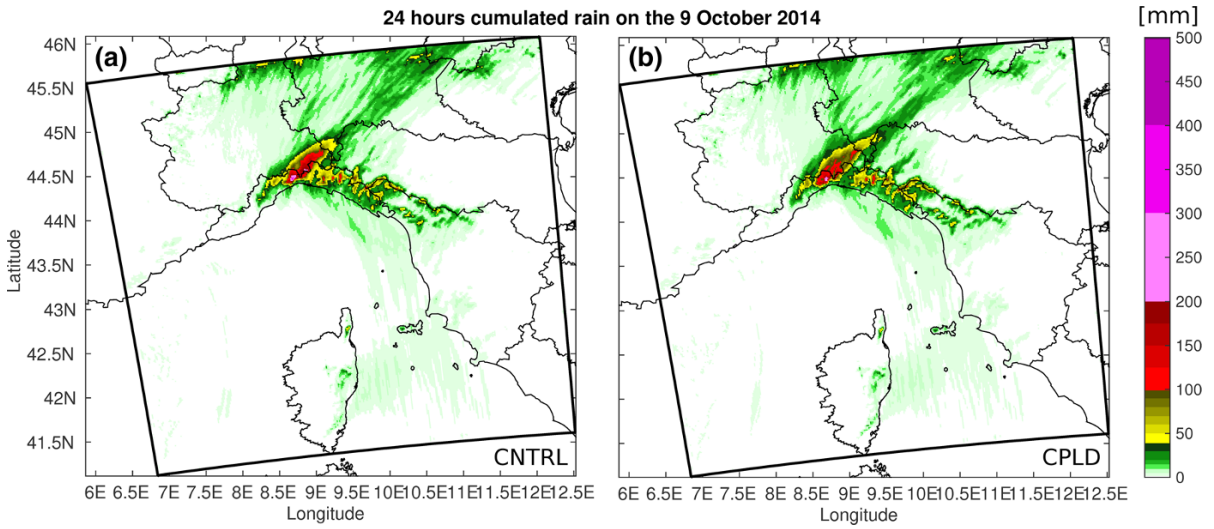


Figure 3

Maps of total rain cumulated over 24 h (mm) on the 9th October in the simulations CNTRL (left panel) and CPLD (right panel)

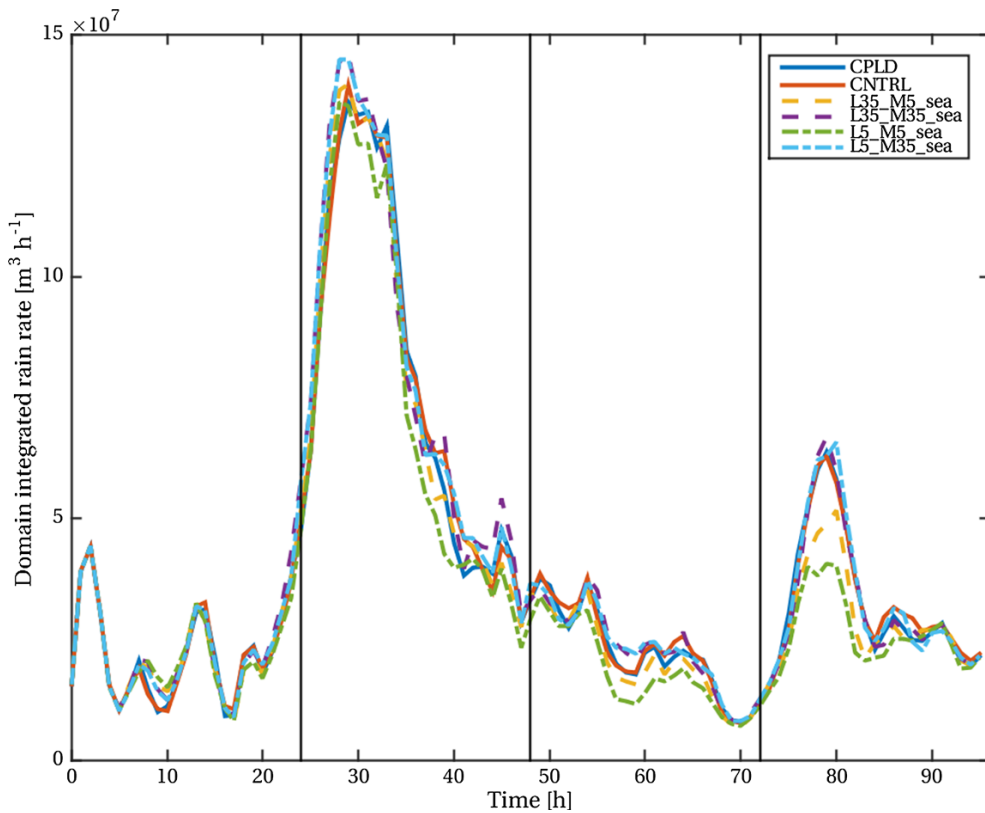


Figure 4

Hourly precipitation rate integrated over the entire domain of the simulation as a function of time. The vertical black lines denote midnight. Two high peaks are visible, one around 0700 UTC 7 October 2014 and the other around 0800 UTC 9 October 2014. The two least-rain-producing simulations are the ones with the shallowest initial mixed layer, L5_M5_sea and L35_M5_sea

time. There is a first high peak of precipitation around 0700 UTC 7 October 2014, which corresponds to a HPE over the sea (Meroni et al. 2018), and then a second peak around 0800 UTC 9 October 2014, which is the heavy rainfall that hit the Bisagno catchment and the City of Genoa. Even if the first peak, which happened only over the sea on the 7th October, is higher than the second one, the focus of the following analysis is on the rainfall of the 9th October because it happened over land and, thus, is more relevant for society. Once again, the coupling with the ocean modifies the evolution of the precipitation so little that the CPLD line is almost indistinguishable from the CNTRL one.

The hypothesis for an explanation of such little influence of the ocean dynamics on the HPE is that the oceanic mixed layer is deep enough that it is able to insulate the stratified (colder) water at its base from the vertical mixing action of the winds. In fact, in a thermally stratified ocean, if the mixing is strong enough to deepen and cool down the mixed layer, then the SST and, together with it, the surface heat fluxes are affected by the presence of a dynamical ocean. Otherwise, if the mixing is confined to the mixed layer, no surface expression of the presence of subsurface heat anomalies can impact the thermodynamics of the atmospheric boundary layer and, thus, the precipitation.

An important process related to the vertical ocean stratification in case of HPEs is the formation of low-salinity lenses where the precipitation is intense (Lebeaupin Brossier and Drobinski 2009; Lebeaupin Brossier et al. 2014). These areas, accompanied by areas of increased surface salinity due to high evaporation caused by the intense winds, affect the vertical stratification and, thus, the ocean thermal response. In what follows, since it is the SST response that ultimately controls the surface fluxes, the salinity effect, even if it is fully accounted for in the dynamics, is no longer discussed. Quantification of the effects of these lenses of water on the stratification and eventually the mixed-layer temperature requires new simulations, in which one could switch off the impact of salinity on density, to evaluate its importance. This is left for subsequent work.

Following the definition of MLD given by Houpert et al. (2015), namely the depth at which the temperature is 0.1 °C colder than the SST, instantaneous maps of MLD can be calculated from the CPLD simulation. Figure 5 shows the MLD at the beginning of the simulation (0000 UTC 6 October 2014) and after 3 days from the beginning, i.e., after 2 days of intense winds but before the day of the HPE (at 0000 UTC 9 October 2014). It is easy to see that qualitatively it has not changed much and, in fact, by calculating its horizontal average over the sea,

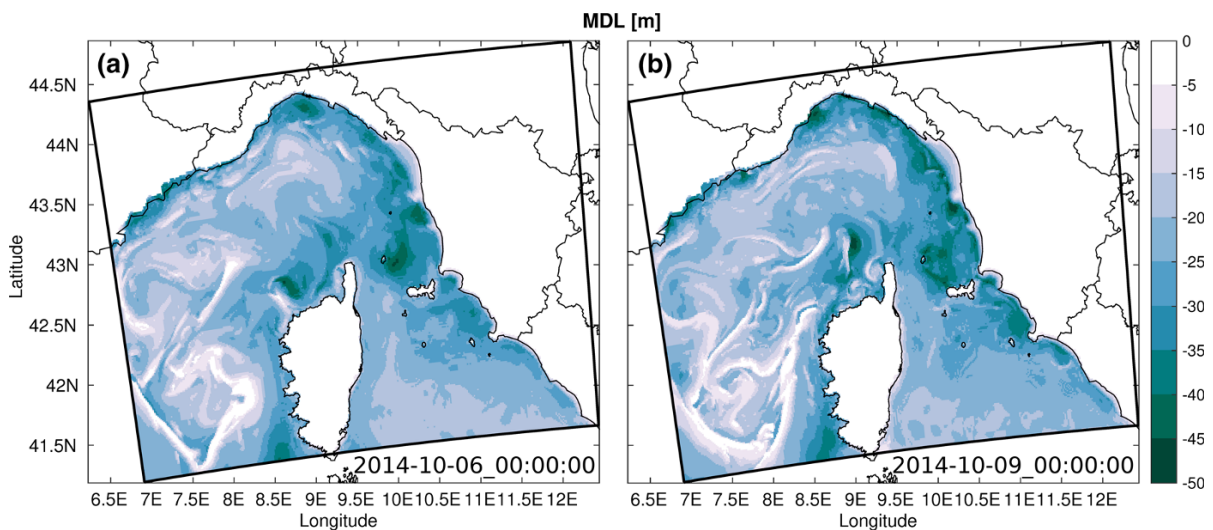


Figure 5

MLD [m] from the CPLD simulation at two different instants: in the left panel at the beginning of the simulation and in the right panel after 3 days, at midnight before the HPE

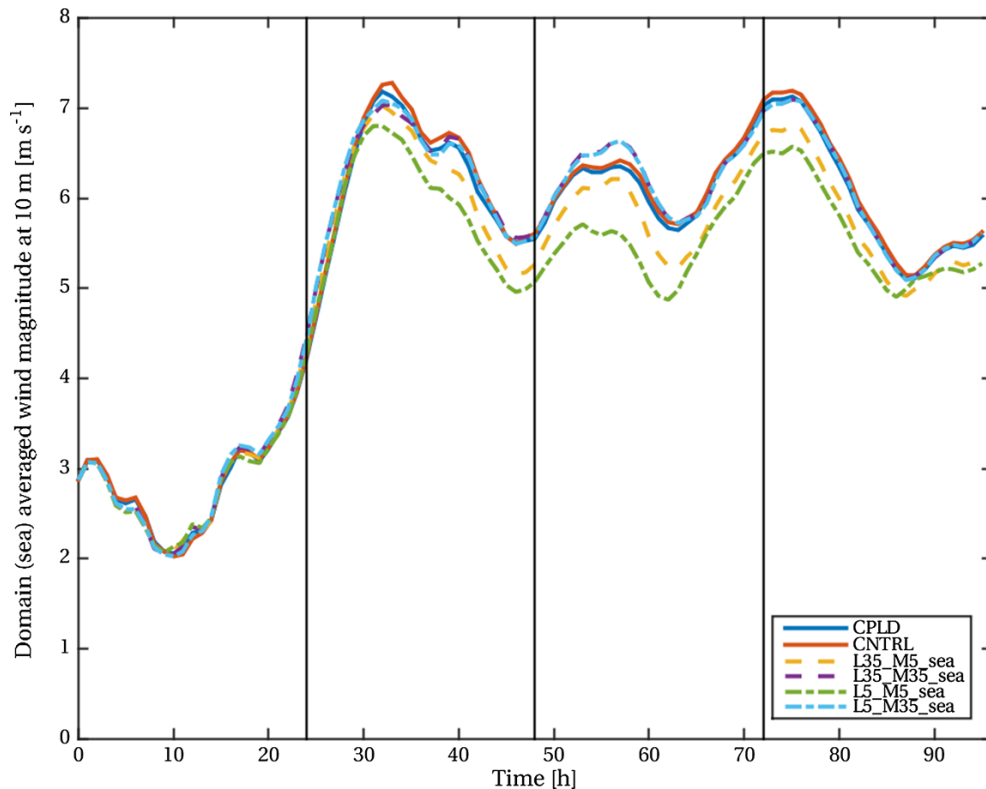


Figure 6

Horizontal average over the sea of the wind magnitude at 10 m over the sea as a function of time for some of the simulations

$$\overline{\text{MLD}} = \frac{1}{|\Omega|} \iint_{\Omega} dx dy \text{MLD}(x, y), \quad (3)$$

one finds that it has changed from $\overline{\text{MLD}} = 21.65$ m at 0000 UTC 6 October 2014 to $\overline{\text{MLD}} = 21.83$ m at 0000 UTC 9 October 2014, much less than the vertical resolution of the grid (a few meters in the upper ocean). Figure 9 also shows that the sea averaged MLD does not change in time throughout the CPLD simulation.

4. Role of the Vertical Oceanic Thermal Structure

4.1. Effects on the SST

The goal of the series of simulations $L^*_M^*_\text{sea}$ is to explore a portion of the parameter space that defines the vertical thermal structure of the ocean, described with the simple potential temperature profile of Eq. (2), to see how the initial state of the ocean can affect the heavy precipitation of a MCS.

Figure 6 shows that the intense winds associated with the synoptic cyclone in which the heavy-rain-producing MCS is embedded start blowing over the domain on the 7th October, a couple of days before the HPE that hit the City of Genoa. To let the ocean respond to the wind forcing that is ahead of the intense rainfall, all the simulations were initialized at 0000 UTC 6 October 2014. The 2 days of intense winds preceding the rainfall peak of the 9th October reduce the average SST in the Ligurian Sea mostly by entrainment in the mixed layer of deeper and colder water. Depending on the initial vertical profile, this effect is more or less pronounced, as shown in Fig. 7, where the daily mean of the SST averaged over the Ligurian Sea is displayed as a function of time for some simulations. For a shallow initial mixed layer ($M = 5$ m), the cooling can be as large as 1°C ($L = 35$ m) or 2°C ($L = 5$ m), while for a deeper initial mixed layer ($M = 35$ m), it can be as small as 0.1°C . The simulation with the highest cooling is the

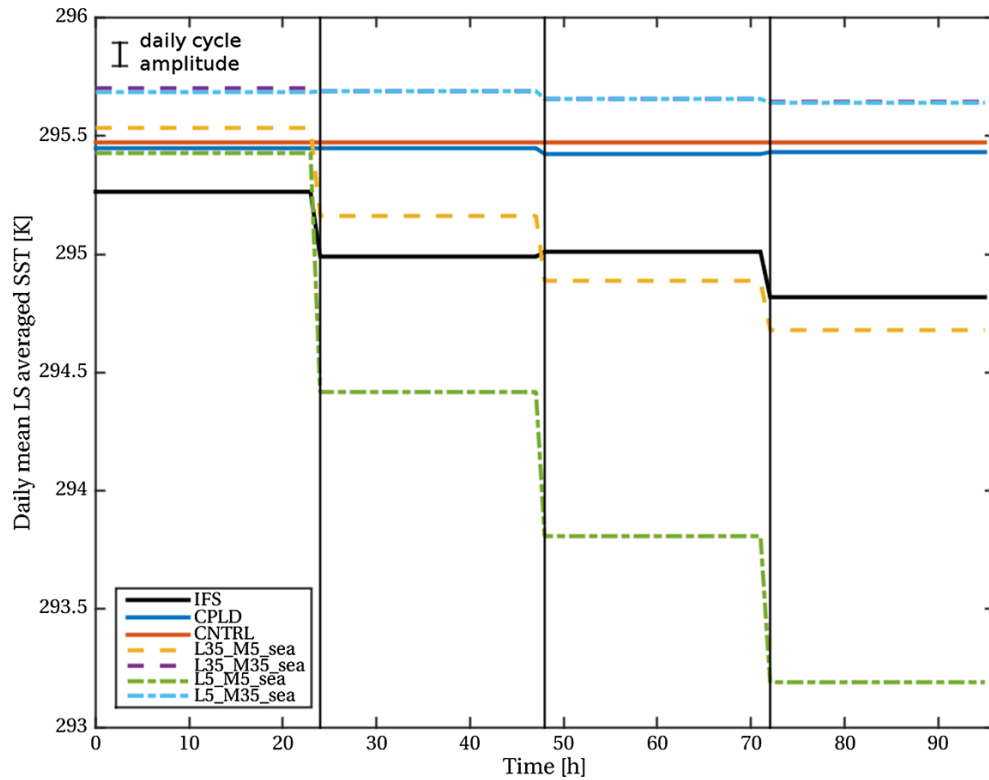


Figure 7

Daily mean of the horizontal average of the SST over the Ligurian Sea (LS) as a function of time for some of the simulations. The average amplitude of the daily cycle (difference between the SST daily maximum and the SST daily minimum) for the CPLD case is shown in the upper left corner

one with the shallowest initial mixed layer ($M = 5$ m) and the strongest stratification ($L = 5$ m).

Another quantity to measure the strength of a vertical ocean profile in opposing the mixing action of the winds was introduced by Vincent et al. (2012): the cooling inhibition (CI) index. It is related to the amount of energy required to mix the upper ocean so that the mixed layer is 2°C colder. For the analytical initial thermal profiles of the series of simulations $L^*_M^*_\text{sea}$, it is found that the CI index increases with increasing M , because the mixed layer gets deeper and deeper for higher M , and increases with increasing L , because the cold water is further down as L increases. It is found, then, that the daily average SST of the Ligurian Sea on the 8th October (on the third day of the simulation, the day preceding the HPE) monotonically increases with the CI index, as in Fig. 8. This indicates that the CI index and the average SST on the 8th October contain the same information on the ocean response: the lower the

energy required to overcome the vertical density profile and to cool the mixed layer (low CI index), the colder the Ligurian sea after 2 days of intense winds (low SST on the 8th October).

A significant reduction of the average surface wind magnitude can be observed in the case of intense SST cooling, by looking at Figs. 6 and 7. This mechanism has been studied in Meroni et al. (2018), where it is highlighted that the mechanism through which the SST controls the surface wind over $O(\text{km})$ spatial scales and over $O(\text{h})$ temporal scales is the downward momentum mixing mechanism. In particular, when an air parcel moves over a relatively warmer sea area, the increased air instability induces vertical mixing, which brings momentum downward. In case of air moving over a relatively colder area, instead, an internal boundary layer characterized by reduced surface wind speed develops (Small et al. 2008).

In the case where the mixed layer is too deep, there is a restratification at the base of the mixed layer

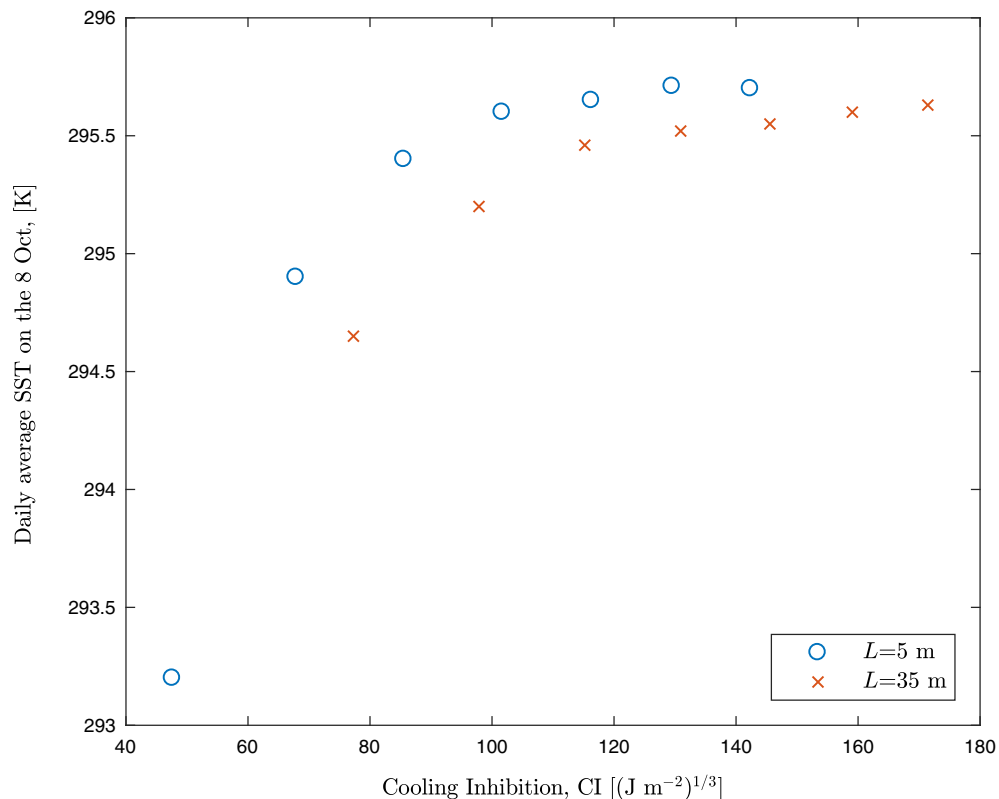


Figure 8

Daily average SST of the Ligurian Sea on the 8th October as a function of the CI index. Since the deeper the initial mixed layer M the higher the CI index (not shown), also the daily average SST on the 8th October increases with M

due to the shear turbulent heat fluxes induced by an imbalance between the current and temperature initial conditions. This restratification causes a shallowing of the mixed layer, because the mixing happens in the upper thermocline, near the temperature interface. Figure 9 supports this interpretation, by showing the daily mean MLD, averaged over the sea as a function of time for some simulations. For a shallow initial mixed layer ($M = 5$ m), the winds are able to deepen it, in particular when the underlying stratification is relatively weak ($L = 35$ m). For a deeper initial mixed layer ($M = 35$ m), the deep and cold water at its base are insulated from the mixing action of the winds and thus the MLD is basically constant, as well as the SST shown in the previous figure. For the case with strong stratification ($L = 5$ m), there is a slight thinning of the MLD during the first simulated day, because of the shear-induced mixing at the sharp temperature vertical gradient at the base of the mixed layer. The CPLD case average MLD does not change

much over the duration of the simulation, which suggests that the winds are not strong enough to affect it, as previously explained.

By looking again at Fig. 7, it is interesting to note that the IFS SST (Simmons et al. 1989), which was used to force the atmospheric model as described in Sect. 2.1, shows a significant reduction over the course of the second day period, while in the coupled simulation, where the mixed layer is about 20 m deep, the average SST reduction is almost one order of magnitude smaller. A SST reduction similar to the IFS one is found for a significantly shallower initial mixed layer (5 m), suggesting that either the winds are underestimated in WRF and/or the ocean vertical mixing scheme does not perform well under these conditions. Another issue that might explain the discrepancy is that the IFS SST has much lower resolution compared with the model. Thus, it is likely that some fine-scale SST structures are

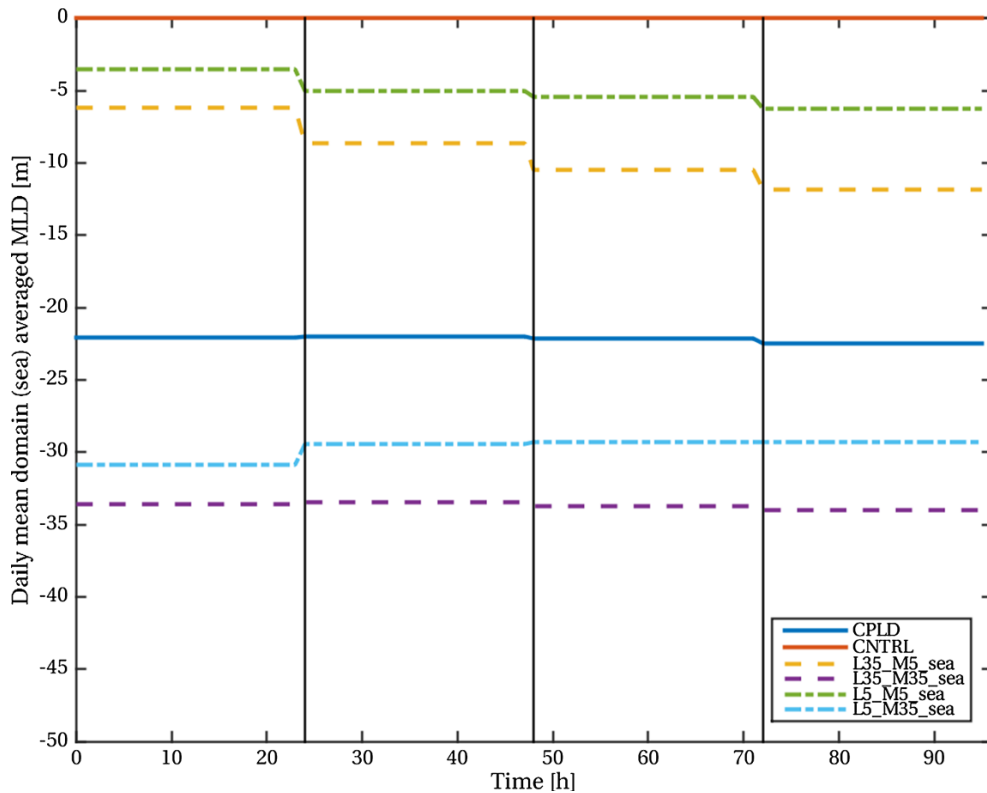


Figure 9

Daily mean of the horizontal average of the MLD over the sea as a function of time for some of the simulations

smoothed out and, thus, the spatial average SST value cannot be compared with the model results.

4.2. Effects on the Precipitation

In Fig. 10, the total rain volume cumulated over the domain on the 9th October is shown as a function of the daily mean (8th October) horizontal average SST over the Ligurian Sea for all the simulations considered, namely CNTRL, CPLD, UNIF, and $L^*_M^*_sea$ with $L \in [5, 35]$ m and $M \in [5, 10, 15, 20, 25, 30, 35]$ m. There is a clear increase in the total precipitation with increasing average SST, as known from Pastor et al. (2001) and Lebeaupin et al. (2006). The underlying trend is estimated to be roughly $1 \times 10^8 \text{ m}^3 \text{ K}^{-1}$, which in percentage terms means that, per degree, the total cumulated rain changes by roughly 10 %, which is in agreement with the findings of Lebeaupin et al. (2006). Since this trend appears to be robust, it was used to find an estimate of the uncertainty on the rain

volume as follows: Consider all the data with SST in the interval $[295.5, 295.7]$ K. Since their standard deviation $\sigma_{rv} = 2 \times 10^7 \text{ m}^3$ is larger than the linear increase due to the background trend in the aforementioned temperature interval, this is taken as an estimate of the spread of the value of the rain volume around the background trend, corresponding to a relative uncertainty of roughly 3 %.

The slight decrease in precipitation between the CNTRL and CPLD simulations, roughly 2 %, thus falls within the uncertainty and is not significant, confirming that the coupled dynamics is not important in this case study. Instead, considering the series of simulations with $L = 35$ m, the reduction of cumulated rain of the case L35_M5_sea with respect to the CNTRL case is around 13 %, while for $L = 5$ m, in the case L5_M5_sea the reduction is roughly 20 %. The cases with the lowest precipitation are the ones where the initial MLD is the shallowest, namely $L = 5$ m, which are also the cases with lowest average SST.

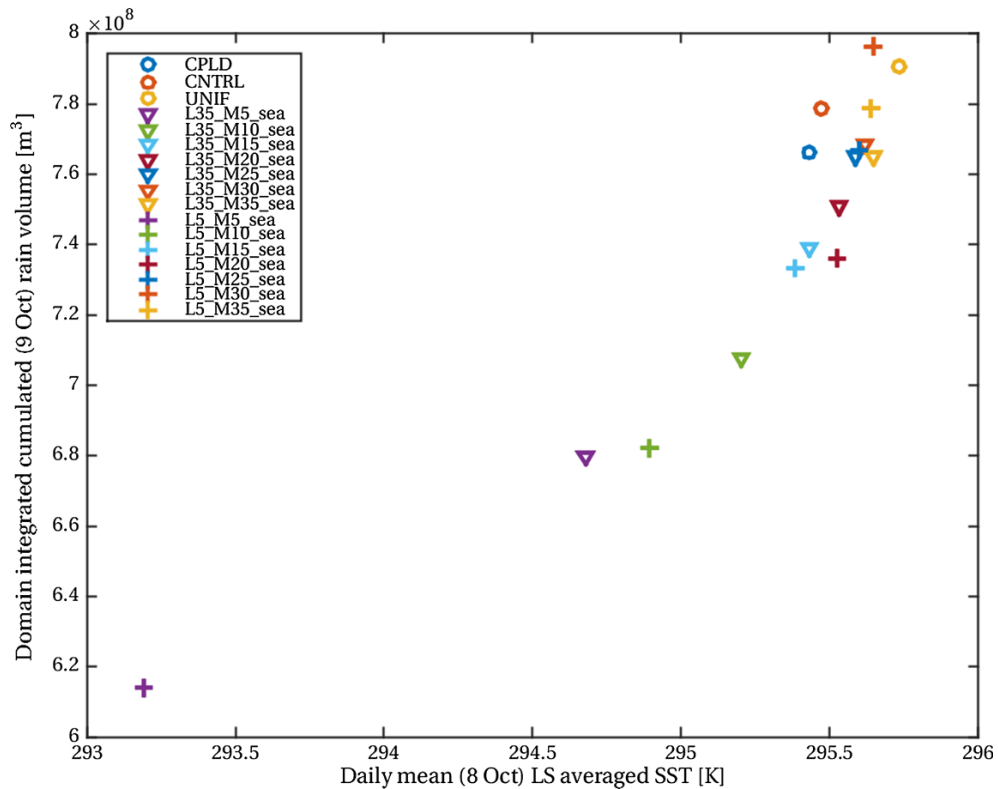


Figure 10

Domain integrated rain volume cumulated on the 9th October as a function of the SST averaged on the Ligurian Sea on the 8th October

Thus, the different initial vertical thermal structures respond to the intense wind forcing preceding the HPE in different ways, generally reducing the SST in the area in the vicinity of the convective rain event, which reduces the air column instability and its ability to produce intense rainfalls. This is proved by Fig. 11, where the maps of the convective available potential energy (CAPE) of the surface air parcel at 0000 UTC 9 October 2014, midnight before the HPE, are shown for two different simulations, L5_M5_sea in the left panel and L5_M35_sea in the right one. The CAPE is calculated here as the integral of the difference between the adiabatic lifted surface air parcel temperature profile and the local temperature profile between the level of free convection and the equilibrium level of the surface air parcel itself. From Fig. 11, it is clear that, for a shallow initial mixed layer ($M = 5$ m, left panel), the CAPE is strongly reduced with respect to a case with a deeper one ($M = 35$ m, right panel).

A closer look at the data of Fig. 10, then, suggests that, when the initial MLD is 25 m or deeper, the average SST is independent of the exact oceanic vertical thermal structure, as indicated by the very similar values of SST for the cases L5_M25, L5_M30, L5_M35, L35_M25, L35_M30, L35_M35, and UNIF. This is indicative of a sort of threshold behavior of the total precipitation as a function of the initial MLD, via the control of the average SST. In fact, when looking at the rain volume cumulated on the 9th October as a function of the initial MLD, as in Fig. 12, it is easy to see that the rain volume first increases and then saturates around $M = 25$ m. The differences between the two series with different values of stratification, L , are within the uncertainty estimated above (except for the case $M = 5$ m) and thus are thought to be caused by some secondary mechanisms.

For example, this might be due to the presence of sharper horizontal SST gradients in the case of small L (stronger stratification), which are known to affect

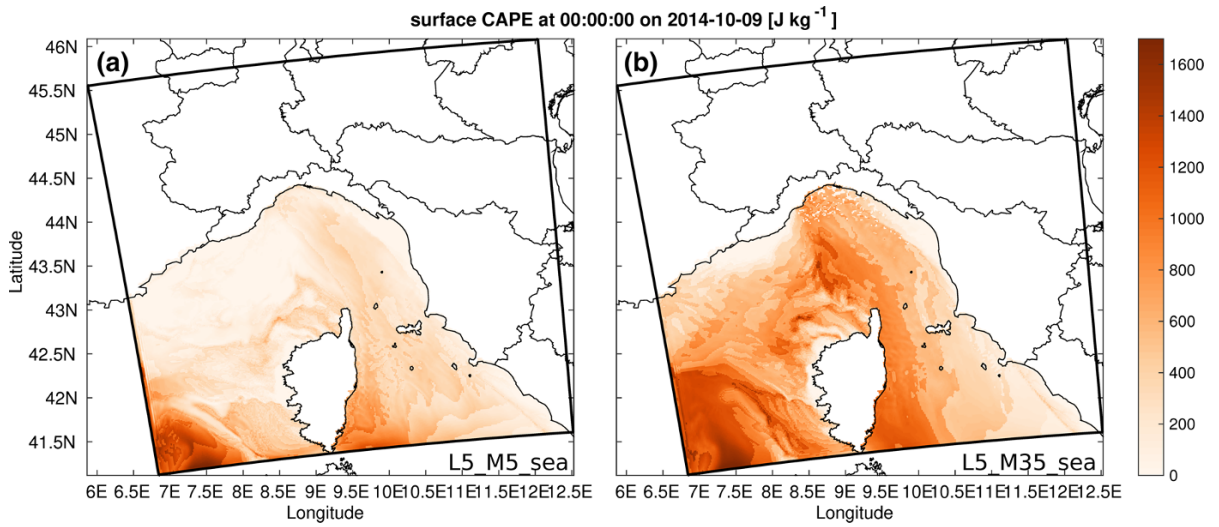


Figure 11

Snapshot of the CAPE [J kg^{-1}] at 0000 UTC 9 October 2014 from the simulations L5_M5_sea (shallow mixed layer) in the left panel and L5_M35_sea (deep mixed layer) in the right panel

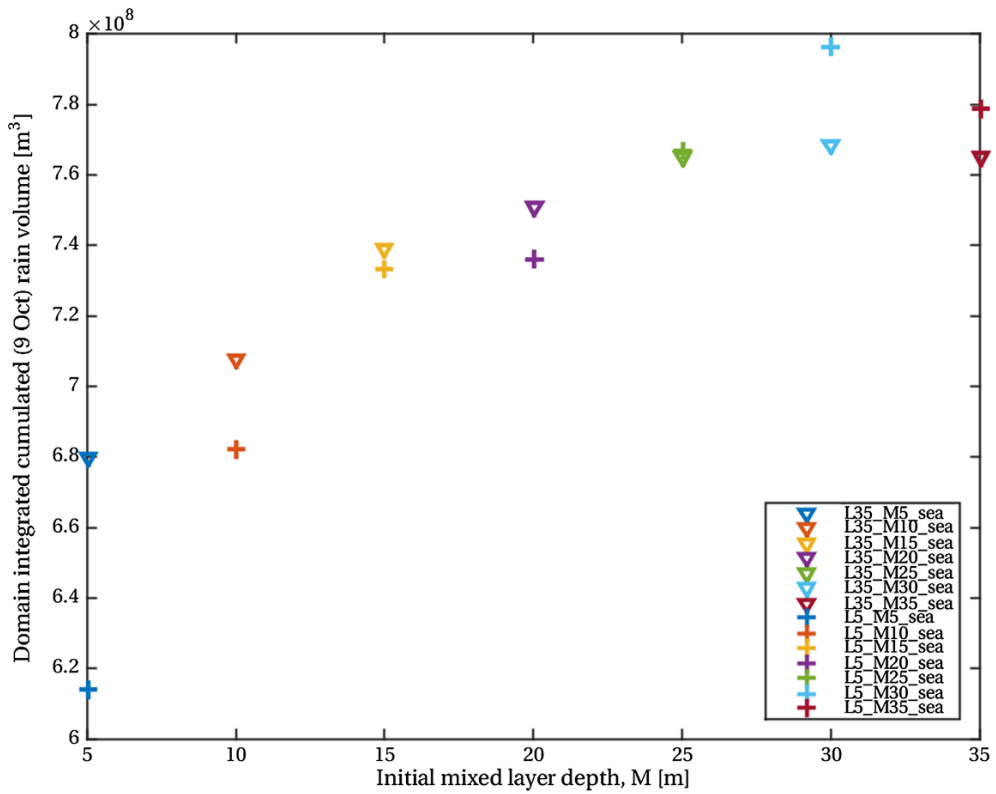


Figure 12

Rain cumulated over 24 h on the 9th October and integrated over the domain as a function of the initial mixed layer depth M . The uncertainty is estimated to be $\sigma_{rv} = 2 \times 10^7 \text{ m}^3$ (see text)

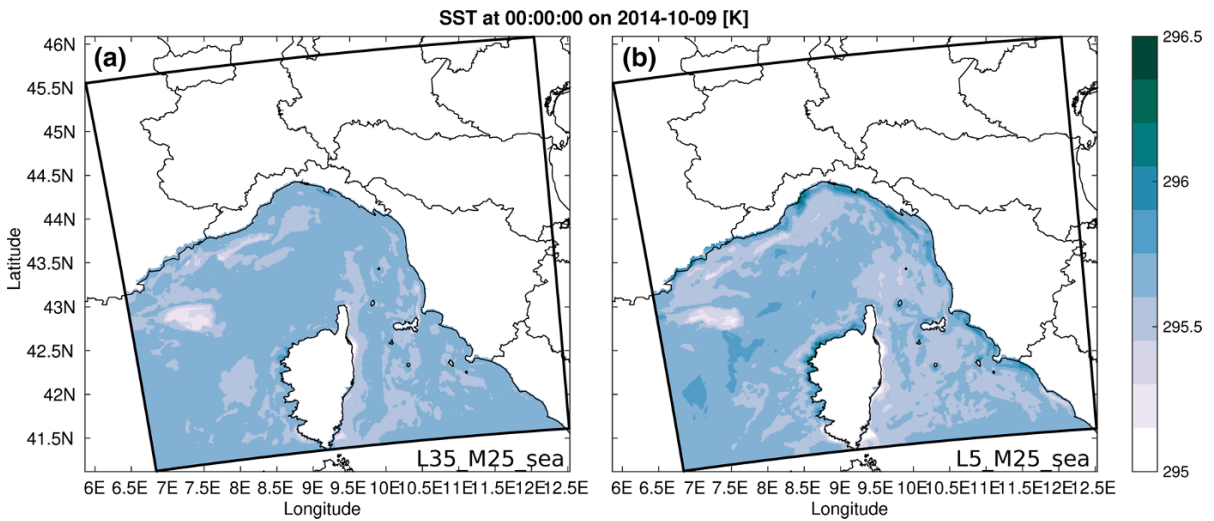


Figure 13

Snapshot of the SST [K] at 0000 UTC 9 October 2014 from the simulations L35_M25_sea (weaker stratification) in the left panel and L5_M25_sea (stronger stratification) in the right panel

the surface wind structures and, possibly, the precipitation field (Meroni et al. 2018), but are not discussed here in detail. In fact, imposing a shorter e-folding length L in the initial temperature profile corresponds to increasing the stratification at the base of the mixed layer. This means that, on the one hand, it is harder to mix the water column, because of the stronger vertical density gradient to overcome, but on the other hand, when the wind is intense enough, the mixing results in stronger surface cooling. Since the winds are not homogeneous over the sea, but have a rapidly changing spatial structure with very fine-scale features, those two effects combined induce relatively sharper horizontal gradients in the SST field after a few days from the initialization of the simulation with relatively stronger stratification. Figure 13 shows this, by displaying the SST field at 0000 UTC 9 October 2014 from the simulations L35_M25_sea (left panel) and L5_M25_sea (right panel). Starting from the same MLD, $M = 25$ m, it is possible to see that, for stronger stratification (small L), the horizontal SST gradients are sharper.

5. Discussion and Conclusions

The mechanism through which the thermal vertical oceanic structure can control the precipitation of a

HPE is found to be the following: For a shallow oceanic mixed layer, the intense winds of the synoptic system that drives the heavy-rain-producing MCS are able to entrain deep and cold water in the mixed layer, resulting in a substantial reduction of the average SST in the region near the HPE, of the order of 1°C . This does not happen if the initial mixed layer is deep enough that the effect of the winds is to mix water within the mixed layer itself. The change in SST, then, is known to control the amount of precipitation (Pastor et al. 2001; Lebeaupin et al. 2006), through, for example, changes in the air column stability.

This suggests that the reason why the coupling with the ocean seems to be totally ineffective in the case study considered is because the MLD in the coupled simulation is deep enough to insulate the colder and deeper water from the mixing action of the winds. Thus, since in the coupled simulation (CPLD) the reduction of the SST with respect to the uncoupled one (CNTRL) is very small, the difference in total precipitation between a case with fully resolved three-dimensional ocean dynamics and a case with a time-independent SST forcing field appears to be negligible. The coupling with the ocean dynamics is more important in the case of shallower mixed layer, as the series of simulations forced with simple vertical temperature profiles, $L^*_M^*_sea$, shows.

Reductions of the total precipitation of roughly 20 % are found in the shallowest mixed layer cases, indicating that the vertical thermal structure of the ocean can considerably reduce the amount of rainfall in such HPEs, in specific conditions.

It is also possible that, since the domain is relatively small, the surface air is already moist and warm and, thus, the surface fluxes are small. If a larger domain were coupled in the simulations, further heat and moisture sources would be included and the coupled dynamics is likely to have a greater impact.

The MLD threshold value that determines whether the ocean dynamics is important or not depends on the magnitude of the winds of the system considered. In this case study, the intense surface winds of the synoptic system driving the HPE have a spatial average magnitude of 6.5 m s^{-1} , with local peak values on the order of 20 m s^{-1} . In other HPEs along the coasts of the Western Mediterranean, e.g., in Lebeaupin et al. (2006), the low-level jet has been observed to reach wind speed of roughly 30 m s^{-1} , suggesting that the range of parameters involved in the mechanism described extends to even stronger wind events. It is suggested that future work should include the development of a physically based definition of the upper ocean heat content that takes into account the intensity and duration of the winds. Similar efforts have been made in the tropical cyclone literature (Miyamoto et al. 2017) with the aim of better predicting the SST anomaly under the eye of the cyclone as per action of the winds.

The conditions that maximize the mitigating effect of the ocean dynamics on the precipitation in such HPEs are typical of the end of the summer, when the first cyclones arrive in the area. In fact, when the ocean has been heated up by the strong summer solar heat flux, it has a shallow mixed layer and strong stratification beneath it (D'Ortenzio et al. 2005; Houpert et al. 2015). In such conditions, the strong winds associated with the heavy-rain-producing MCS can mix up cold water, which is relatively close to the surface, and the colder SST can feed back on the MCS, reducing its instability and, thus, the total cumulated rain. When, then, in autumn, stronger winds deepen the mixed layer, the ability of the sea to reduce the lower atmosphere instability through a

colder SST is attenuated. As a consequence, this might partially explain the timing of such HPEs, which do not generally happen right at the end of the summer, but in mid and late autumn. To test that this is the case, it is indeed desirable to carry out similar analysis on other case studies, with different synoptic conditions and different upper ocean thermal structure.

It is also important to underline that this work was not intended to improve the forecast of these heavy-rain-producing MCSs, but to understand more about the importance of the vertical thermal structure of the upper ocean in the control of such HPEs. This is the reason why the analysis of the results is not invalidated by some of the biases of the model, such as the absence of rain over the sea on the 9th of October or the underestimation of the surface cooling in the coupled ocean–atmosphere simulation with respect to what happened in reality. In fact, the reasons for such biases are known (choice of initialization and difficulty in resolving the very small wind structures or vertical mixing parameterization), as explained in the previous sections, and do not affect the mechanism described above.

The mechanism of acceleration (deceleration) of the surface wind due to relatively warmer (colder) sea surface temperature (Meroni et al. 2018) is found to accentuate the role of negative feedback of the ocean–atmosphere coupled dynamics. In fact, if over a warmer sea area the wind is accelerated, because of vertical mixing in the atmosphere due to higher instability that brings momentum downward, the ocean vertical mixing is also enhanced, so that the SST is reduced. To properly tackle this problem, a simplified setup might be more appropriate.

It is left for future work to include, then, the effect of wave dynamics. It is known, in fact, that a wave model improves the representation of surface fluxes (Carniel et al. 2016; Ricchi et al. 2016, 2017). In particular, in case of relatively strong winds (stronger than 10 m s^{-1}), inclusion of wave dynamics is important in the modulation of the air–sea momentum exchanges, because of the increased surface roughness (Thévenot et al. 2016). This determines an increased transfer of momentum from the atmosphere to the ocean, which determines an increase in the

effectiveness of vertical ocean mixing, with subsequent surface cooling.

Finally, targeted analysis on the role of the salinity effect on the ocean stratification and, thus, on the HPE dynamics is encouraged. In fact, the Northwestern Mediterranean is characterized by the presence of both surface salinity gradients, due to the large evaporation in the Gulf of Lion, and vertical variations due to differences in water masses, namely Atlantic Water is above Levantine Intermediate Water, which is above Western Mediterranean Dense Water (Millot and Taupier-Letage 2005). These realistic salinity structures, together with the formation of low-salinity lenses in the areas of intense rain (Lebeaupin Brossier and Drobinski 2009; Lebeaupin Brossier et al. 2014), which have already been included in the dynamics of the present work, are planned to be the object of future detailed analysis.

Acknowledgements

A.N.M. is funded by the Flagship Project RIT-MARE—the Italian Research for the Sea—coordinated by the Italian National Research Council and funded by the Italian Ministry of Education, University, and Research within the National Research Program 2011–2013. L.R. is supported by the National Science Foundation (OCE-1419450). A.P. is supported by the Italian Civil Protection Department and by the Regione Liguria. This article is an outcome of Project MIUR – Dipartimenti di Eccellenza 2018–2022. The authors are grateful for the careful revision by the anonymous reviewers, which led to substantial improvements to the manuscript.

REFERENCES

Beckmann, A., & Haidvogel, D. B. (1993). Numerical simulation of flow around a tall isolated seamount. Part I: Problem formulation and model accuracy. *Journal of Physical Oceanography*, 23, 1736–1753. [https://doi.org/10.1175/1520-0485\(1993\)023%3c1736:NSOFAA%3e2.0.CO;2](https://doi.org/10.1175/1520-0485(1993)023%3c1736:NSOFAA%3e2.0.CO;2).

Beljaars, A. C. M. (1995). The parameterization of surface fluxes in large-scale models under free convection. *Quarterly Journal of the Royal Meteorological Society*, 121, 255–270.

Berthou, S., Mailler, S., Drobinski, P., Arsouze, T., Bastin, S., Béranger, K., et al. (2015). Sensitivity of an intense rain event

between atmosphere-only and atmosphere-ocean regional coupled models: 19 September 1996. *Quarterly Journal of the Royal Meteorological Society*, 141, 258–271. <https://doi.org/10.1002/qj.2355>.

Buzzi, A., Davolio, S., Malguzzi, P., Drofa, O., & Mastrangelo, D. (2014). Heavy rainfall episodes over Liguria in autumn 2011: Numerical forecasting experiments. *Natural Hazards and Earth System Sciences*, 14(5), 1325–1340. <https://doi.org/10.5194/nhess-14-1325-2014>.

Carniel, S., Benetazzo, A., Bonaldo, D., Falcieri, F. M., Miglietta, M. M., Ricchi, A., et al. (2016). Scratching beneath the surface while coupling atmosphere, ocean and waves: Analysis of a dense water formation event. *Ocean Modelling*, 101, 101–112. <https://doi.org/10.1016/j.ocemod.2016.03.007>.

Cassola, F., Ferrari, F., & Mazzino, A. (2015). Numerical simulations of Mediterranean heavy precipitation events with the WRF model: A verification exercise using different approaches. *Atmospheric Research*, 164–165, 210–225. <https://doi.org/10.1016/j.atmosres.2015.05.010>.

Cassola, F., Ferrari, F., Mazzino, A., & Miglietta, M. M. (2016). The role of the sea in the flash floods events over Liguria (northwestern Italy). *Geophysical Research Letters*, 43, 3534–3542. <https://doi.org/10.1002/2016GL068265>.

Chou, M. D., & Suarez, M. J. (1999). A solar radiation parameterization for atmospheric studies. *NASA Technical Memorandum*, 104606, 15.

Chou, M. D., Suarez, M. J., Liang, X. Z., & Yan, M. M. H. (2001). A thermal infrared radiation parameterization for atmospheric studies. *NASA Technical Memorandum*, 104606, 19.

De Zolt, S., Lionello, P., Nuhu, A., & Tomasin, A. (2006). The disastrous storm of 4 November 1966 in Italy. *Natural Hazards and Earth System Science*, 6, 861–879. <https://doi.org/10.5194/nhess-6-861-2006>.

Debreu, L., Marchesiello, P., Penven, P., & Cambon, G. (2012). Two-way nesting in split-explicit ocean models: Algorithms, implementation and validation. *Ocean Modelling*, 49, 1–21.

D'Ortenzio, F., Iudicone, D., de Boyer, Montegut C., Testor, P., Antoine, D., Marullo, S., et al. (2005). Seasonal variability of the mixed layer depth in the Mediterranean Sea as derived from in situ profiles. *Geophysical Research Letters*, 32, L12605. <https://doi.org/10.1029/2005GL022463>.

Ducrocq, V., Braud, I., Davolio, S., Ferretti, R., Flamant, C., Jansa, A., et al. (2014). HyMeX-SOP1: The field campaign dedicated to heavy precipitation and flash flooding in the northwestern Mediterranean. *Bulletin of the American Meteorological Society*, 95, 1083–1100. <https://doi.org/10.1175/BAMS-D-12-00244.2>.

Dudhia, J. (1996). A multi-layer soil temperature model for MM5. The sixth PSU/NCAR Mesoscale Model users' workshop.

Duffourg, F., Nuissier, O., Ducrocq, V., Flamant, C., Chazette, P., Delanoë, J., et al. (2016). Offshore deep convection initiation and maintenance during the HyMeX IOP 16a heavy precipitation event. *Quarterly Journal of the Royal Meteorological Society*, 142, 259–274. <https://doi.org/10.1002/qj.2725>.

Faccini, F., Luino, F., Paliaga, G., Sacchini, A., & Turconi, L. (2015). Yet another disaster flood of the Bisagno stream in Genoa (Liguria, Italy): October the 9th–10th 2014 event. *Rendiconti Online della Società Geologica Italiana*, 35, 128–131. <https://doi.org/10.3301/ROL.2015.81>.

Fairall, C. W., Bradley, E. F., Hare, J. E., Grachev, A. A., & Edson, J. B. (2003). Bulk parameterization of air-sea fluxes: Updates and verification for the COARE algorithm. *Journal of Climate*, 16,

- 571–591. [https://doi.org/10.1175/1520-0442\(2003\)016%3c0571:BPOASF%3e2.0.CO;2](https://doi.org/10.1175/1520-0442(2003)016%3c0571:BPOASF%3e2.0.CO;2).
- Fiori, E., Comellas, A., Molini, L., Reborá, N., Siccardi, F., Gochis, D. J., et al. (2014). Analysis and hindcast simulations of an extreme rainfall event in the Mediterranean area: The Genoa 2011 case. *Atmospheric Research*, *138*, 13–29.
- Fiori, E., Ferraris, L., Molini, L., Siccardi, F., Kranzlmüller, D., & Parodi, A. (2017). Triggering and evolution of a deep convective system in the Mediterranean Sea: Modelling and observations at a very fine scale. *Quarterly Journal of the Royal Meteorological Society*, *143*, 927–941. <https://doi.org/10.1002/qj.2977>.
- Flamant, C. (2003). Alpine lee cyclogenesis influence on air-sea heat exchanges and marine atmospheric boundary layer thermodynamics over the western Mediterranean during a Tramontane/Mistral event. *Journal of Geophysical Research: Oceans*. <https://doi.org/10.1029/2001JC001040>.
- Gaume, E., Bain, V., Bernardara, P., Newinger, O., Barbuc, M., Bateman, A., et al. (2009). A compilation of data on European flash floods. *Journal of Hydrology*, *367*, 70–78.
- Hong, S. Y., & Lim, J. O. J. (2006). The WRF single moment 6-class microphysics scheme (WSM6). *Journal of the Korean Meteorological Society*, *42*, 129–151.
- Houpert, L., Testor, P., Durrieu de Madron, X., Somot, S., D'Ortenzio, F., Estournel, C., et al. (2015). Seasonal cycle of the mixed layer, the seasonal thermocline and the upper-ocean heat storage rate in the Mediterranean Sea derived from observations. *Progress in Oceanography*, *132*, 333–352. <https://doi.org/10.1016/j.pocean.2014.11.004>.
- Jackett, D. R., & McDougall, T. (1995). Minimal adjustment of hydrographic profiles to achieve static stability. *Journal of Atmospheric and Oceanic Technology*, *12*, 381–389.
- Jacob, D., Petersen, J., Eggert, B., Alias, A., Christensen, O. B., Bouwer, L. M., et al. (2014). Euro-CORDEX: New high-resolution climate change projections for European impact research. *Regional Environmental Change*, *14*, 563–578. <https://doi.org/10.1007/s10113-013-0499-2>.
- Juza, M., Mourre, B., Renault, L., Gómara, S., Sebastián, K., Lora, S., et al. (2016). SOCIB operational ocean forecasting system and multi-platform validation in the Western Mediterranean Sea. *Journal of Operational Oceanography*, *9*, s155–s166.
- Lagasio, M., Parodi, A., Procopio, R., Rachidi, F., & Fiori, E. (2017). Lightning potential index performances in multimicrophysical cloud-resolving simulations of a back-building mesoscale convective system: The Genoa 2014 event. *Journal of Geophysical Research: Atmospheres*, *122*(8), 4238–4257. <https://doi.org/10.1002/2016JD026115>.
- Large, W. G., McWilliams, J. C., & Doney, S. C. (1994). Oceanic vertical mixing: A review and a model with a nonlocal boundary layer parametrization. *Reviews of Geophysics*, *32*, 363–403.
- Lebeaupin, C., Ducrocq, V., & Giordani, H. (2006). Sensitivity of torrential rain events to the sea surface temperature based on high-resolution numerical forecasts. *Journal of Geophysical Research*, *111*, D12110. <https://doi.org/10.1029/2005JD006541>.
- Lebeaupin Brossier, C., & Drobinski, P. (2009). Numerical high resolution air-sea coupling over the Gulf of Lions during two Tramontane/Mistral events. *Journal of Geophysical Research*, *114*, D10110. <https://doi.org/10.1029/2008JD011601>.
- Lebeaupin Brossier, C., Drobinski, P., Béranger, K., Bastin, S., & Orain, F. (2013). Ocean memory effect on the dynamics of coastal heavy precipitation preceded by a mistral event in the northwestern Mediterranean. *Quarterly Journal of the Royal Meteorological Society*, *139*, 1583–1597. <https://doi.org/10.1007/s10236-011-0502-8>.
- Lebeaupin Brossier, C., Arsouze, T., Béranger, K., Bouin, M. N., Bresson, E., Ducrocq, V., et al. (2014). Ocean mixed layer responses to intense meteorological events during HyMeX-SOP1 from a high-resolution ocean simulation. *Ocean Modelling*, *84*, 84–103. <https://doi.org/10.1016/j.ocemod.2014.09.009>.
- Lemarié, F., Debreu, L., Shchepetkin, A. F., & McWilliams, J. C. (2012). On the stability and accuracy of the harmonic and biharmonic isoneutral mixing operators in ocean models. *Ocean Modelling*, *52–53*, 9–35. <https://doi.org/10.1016/j.ocemod.2012.04.007>.
- Lionello, P., Martucci, G., & Zampieri, M. (2003). Implementation of a coupled atmosphere-wave-ocean model in the Mediterranean sea: Sensitivity of the short time scale evolution to the air-sea coupling mechanisms. *Journal of Atmospheric & Ocean Science*, *9*(1–2), 65–95. <https://doi.org/10.1080/1023673031000151421>.
- Llasat, M. C., Llasat-Botija, M., Petrucci, O., Pasqua, A. A., Rosselló, J., Vinet, F., et al. (2013). Towards a database on societal impact of Mediterranean floods within the framework of the HYMEX project. *Natural Hazards and Earth System Sciences*, *13*, 1337–1350. <https://doi.org/10.5194/nhess-13-1337-2013>.
- Marchesiello, P., Debreu, L., & Couvelard, X. (2009). Spurious diapycnal mixing in terrain-following coordinate models: The problem and a solution. *Ocean Modelling*, *26*, 156–169. <https://doi.org/10.1016/j.ocemod.2008.09.004>.
- Mei, W., Xie, S. P., Primeau, F., McWilliams, J. C., & Pasquero, C. (2015). Northwestern Pacific typhoon intensity controlled by changes in ocean temperatures. *Science Advances*, *1*(4), e1500014. <https://doi.org/10.1126/sciadv.1500014>.
- Meroni, A. N., Parodi, A., & Pasquero, C. (2018). Role of SST patterns on surface wind modulation of a heavy midlatitude precipitation event. *Journal of Geophysical Research: Atmospheres*, *123*, 9081–9096. <https://doi.org/10.1029/2018JD028276>.
- Miglietta, M. M., Mazon, J., Motola, V., & Pasini, A. (2017). Effect of a positive sea surface temperature anomaly on a Mediterranean tornadic supercell. *Scientific Reports*, *7*, 12828. <https://doi.org/10.1038/s41598-017-13170-0>.
- Millán, M. M., Estrela, J., & Caselles, V. (1995). Torrential precipitations on the Spanish east coast: The role of the Mediterranean sea-surface temperature. *Atmospheric Research*, *36*, 1–16.
- Millot, C., & Taupier-Letage, I. (2005). Circulation in the Mediterranean Sea. In: Saliot A (ed) *The Mediterranean Sea*, vol. 5, Springer, Berlin, pp. 29–66. <https://doi.org/10.1007/b107143>.
- Miyamoto, Y., Bryan, G. H., & Rotunno, R. (2017). An analytical model of maximum potential intensity for tropical cyclones incorporating the effect of ocean mixing. *Geophysical Research Letters*, *44*, 5826–5835. <https://doi.org/10.1002/2017GL073670>.
- Mlawer, E., Steven, J., Taubman, J., Brown, P. D., Iacono, M. J., & Clough, S. A. (1997). Radiative transfer for inhomogeneous atmospheres: RRTM, a validated correlated-k model for the longwave. *Journal of Geophysical Research*, *102*, 16663–16682.
- Nakanishi, M., & Niino, H. (2006). An improved Mellor–Yamada level 3 model: Its numerical stability and application to a regional prediction of advecting fog. *Boundary-Layer Meteorology*, *119*, 397–407.

- Nakanishi, M., & Niino, H. (2009). Development of an improved turbulence closure model for the atmospheric boundary layer. *Journal of the Meteorological Society of Japan*, *87*, 895–912.
- Nuissier, O., Ducrocq, V., Ricard, D., Lebeaupin, C., & Anquetin, S. (2008). A numerical study of three catastrophic precipitating events over southern France. I: Numerical framework and synoptic ingredients. *Quarterly Journal of the Royal Meteorological Society*, *134*, 111–130. <https://doi.org/10.1002/qj.200>.
- Oddo, P., Adani, M., Pinardi, N., Fratianni, C., Tonani, M., & Pettenuzzo, D. (2009). A nested Atlantic-Mediterranean Sea general circulation model for operational forecasting. *Ocean Science*, *5*, 461–473. <https://doi.org/10.5194/os-5-461-2009>.
- Orlanski, I. (1976). A simple boundary condition for unbounded hyperbolic flows. *Journal of Computer Science*, *21*(3), 251–269.
- Pastor, F., Estrela, M. J., narrocha, D. P., & Millán, M. M. (2001). Torrential rains on the Spanish Mediterranean coast: Modeling the effects of the sea surface temperature. *Journal of Applied Meteorology*, *40*, 1180–1195.
- Penven, P., Debreu, L., Marchesiello, P., & McWilliams, J. C. (2006). Evaluation and application of the ROMS 1-way embedding procedure to the central California upwelling system. *Ocean Modelling*, *12*, 157–187.
- Raymond, W. H., & Kuo, H. L. (1984). A radiation boundary condition for multi-dimensional flows. *Quarterly Journal of the Royal Meteorological Society*, *110*, 535–551.
- Rebora, N., Molini, L., Casella, E., Comellas, A., Fiori, E., Pignone, F., et al. (2013). Extreme rainfall in the Mediterranean: What can we learn from observations? *Journal of Hydrometeorology*, *14*, 906–922. <https://doi.org/10.1175/JHM-D-12-083.1>.
- Ricchi, A., Miglietta, M. M., Falco, P. P., Benetazzo, A., Bonaldo, D., Bergamasco, A., et al. (2016). On the use of a coupled-ocean-atmosphere-wave model during an extreme cold air outbreak over the Adriatic Sea. *Atmospheric Research*, *172–173*, 48–65. <https://doi.org/10.1016/j.atmosres.2015.12.023>.
- Ricchi, A., Miglietta, M. M., Barbariol, F., Benetazzo, A., Bergamasco, A., Bonaldo, D., et al. (2017). Sensitivity of a Mediterranean tropical-like cyclone to different model configurations and coupling strategies. *Atmosphere*, *8*, 92. <https://doi.org/10.3390/atmos8050092>.
- Sandwell, D. T., & Smith, W. H. F. (1997). Marine gravity anomaly from Geosat and ERS 1 satellite altimetry. *Journal of Geophysical Research*, *102*, 10039–10054. <https://doi.org/10.1029/96JB03223>.
- Schade, L. R., & Emanuel, K. A. (1999). The ocean's effect on the intensity of tropical cyclones: Results from a simple coupled atmosphere-ocean model. *Journal of the Atmospheric Sciences*, *56*, 642–651.
- Schumacher, R. S., & Johnson, R. H. (2005). Organization and environmental properties of extreme-rain-producing mesoscale convective systems. *Monthly Weather Review*, *133*, 961–976.
- Schumacher, R. S., & Johnson, R. H. (2008). Mesoscale processes contributing to extreme rainfall in a midlatitude warm-season flash-flood. *Monthly Weather Review*, *136*, 3964–3986.
- Schumacher, R. S., & Johnson, R. H. (2009). Quasi-stationary, extreme-rain-producing convective systems associated with midlevel cyclonic circulations. *Weather and Forecasting*, *24*, 555–574.
- Shchepetkin, A. F. (2015). An adaptive, Courant-number-dependent implicit scheme for vertical advection in oceanic modeling. *Ocean Modelling*, *91*, 38–69. <https://doi.org/10.1016/j.ocemod.2015.03.006>.
- Shchepetkin, A. F., & McWilliams, J. C. (1998). Quasi-monotone advection schemes based on explicit locally adaptive dissipation. *Monthly Weather Review*, *126*, 1541–1580. [https://doi.org/10.1175/1520-0493\(1998\)126%3c1541:QMASBO%3e2.0.CO;2](https://doi.org/10.1175/1520-0493(1998)126%3c1541:QMASBO%3e2.0.CO;2).
- Shchepetkin, A. F., & McWilliams, J. C. (2003). A method for computing horizontal pressure-gradient force in an oceanic model with a nonaligned vertical coordinate. *Journal of Geophysical Research: Oceans*, *108*, 1. <https://doi.org/10.1029/2001JC001047>.
- Shchepetkin, A. F., & McWilliams, J. C. (2009). Correction and commentary for “Ocean forecasting in terrain-following coordinates: Formulation and skill assessment of the regional ocean modeling system” by Haidvogel et al., *J. Comp. Phys.* 227:3595–3624. *Journal of Computational Physics*, *228*, 3595–3624. <https://doi.org/10.1016/j.jcp.2009.09.002>.
- Silvestro, F., Rebora, N., Giannoni, F., Cavallo, A., & Ferraris, L. (2016). The flash flood of the Bisagno creek on 9th October 2014: an “unfortunate” combination of spatial and temporal scales. *Journal of Hydrology*, *541*, 50–62. <https://doi.org/10.1016/j.jhydrol.2015.08.004>.
- Simmons, A. J., Burridge, D. M., Jarraud, M., Girard, C., & Wergen, W. (1989). The ECMWF medium-range prediction models development of the numerical formulations and the impact of increased resolution. *Meteorology and Atmospheric Physics*, *40*, 28–60.
- Skamarock, W.C., Klemp, J.B., Dudhia, J., Gill, D.O., Barker, D.M., Duda, M., et al. (2008). A description of the advanced research WRF version 3. NCAR Tech Note NCAR/TN-475+STR p. <https://doi.org/10.5065/D68S4MVH>.
- Smagorinsky, J. (1963). General circulation experiments with the primitive equations: I. The basic equations. *Monthly Weather Review*, *91*, 99–164.
- Small, R. J., deSzoeke, S. P., Xie, S. P., O'Neilland, H., Seo, L., Song, Q., et al. (2008). Air-sea interaction over ocean fronts and eddies. *Dynamics of Atmospheres and Oceans*, *45*, 274–319. <https://doi.org/10.1016/j.dynatmoce.2008.01.001>.
- Small, R. J., Campbell, T., Teixeira, J., Carniel, S., Smith, T. A., Dykes, J., et al. (2011). Air-sea interaction in the Ligurian Sea: Assessment of a coupled ocean-atmosphere model using in situ data from LASIE07. *Monthly Weather Review*, *139*, 1785–1808. <https://doi.org/10.1175/2010MWR3431.1>.
- Small, R. J., Carniel, S., Campbell, T., Teixeira, J., & Allard, R. (2012). The response of the Ligurian and Tyrrhenian Seas to a summer Mistral event: A coupled atmosphere-ocean approach. *Ocean Modelling*, *48*, 30–44. <https://doi.org/10.1016/j.ocemod.2012.02.003>.
- Stocchi, P., & Davolio, S. (2017). Intense air-sea exchanges and heavy orographic precipitation over Italy: The role of Adriatic sea surface temperature uncertainty. *Atmospheric Research*, *196*, 62–82.
- Thévenot, O., Bouin, M. N., Ducrocq, V., Lebeaupin Brossier, C., On, J., & PianezzeDuffourg, F. (2016). Influence of the sea state on Mediterranean heavy precipitation: a case-study from HyMeX SOP1. *Quarterly Journal of the Royal Meteorological Society*, *142*(S1), 377–389.
- Tiedtke, M. (1989). A comprehensive mass flux scheme for cumulus parameterization in large-scale models. *Monthly Weather Review*, *117*, 1779–1800.
- Valcke, S. (2013). The OASIS3 coupler: A European climate modelling community software. *Geoscientific Model Development*, *6*, 373–388. <https://doi.org/10.5194/gmd-6-373-2013>.

- Vincent, E. M., Lengaigne, M., Vialard, J., Madec, G., Jourdain, N. C., & Masson, S. (2012). Assessing the oceanic control on the amplitude of sea surface cooling induced by tropical cyclones. *Journal of Geophysical Research*, *117*, C05023. <https://doi.org/10.1029/2011JC007705>.
- Zhang, C., Wang, Y., & Hamilton, K. (2011). Improved representation of boundary layer clouds over the southeast Pacific in ARW-WRF using a modified Tiedtke cumulus parameterization scheme. *Monthly Weather Review*, *139*, 3489–3513.

(Received September 28, 2017, revised August 3, 2018, accepted September 21, 2018, Published online October 8, 2018)